2006

Growth of Ge Quantum Dots on Si(100)-(2×1) by Pulsed Laser Deposition

M. S. Hegazy
Old Dominion University

H. E. Elsayed-Ali
Old Dominion University, helsayed@odu.edu

Growth of Ge quantum dots on Si(100)-(2×1) by pulsed laser deposition

M. S. Hegazy and H. E. Elsayed-Ali[a)]
Department of Electrical and Computer Engineering and the Physical Electronics Research Institute,
Old Dominion University, Norfolk, Virginia 23529

Self-assembled germanium quantum dots (QDs) were grown on Si(100)-(2×1) by pulsed laser deposition. *In situ* reflection-high energy electron diffraction (RHEED) and postdeposition atomic force microscopy are used to study the growth of the QDs. Several films of different thicknesses were grown at a substrate temperature of 400 °C using a *Q*-switched Nd:yttrium aluminum garnet laser ($\lambda = 1064$ nm, 40 ns pulse width, 23 J/cm^2 fluence, and 10 Hz repetition rate). At low film thicknesses, hut clusters that are faceted by different planes, depending on their height, are observed after the completion of the wetting layer. With increasing film thickness, the size of the clusters grows and they gradually lose their facetation and become more rounded. With further thickness increase, the shape of these clusters becomes domelike with some pyramids observed among the majority of domes. The effect of the laser fluence on the morphology of the grown clusters was studied. The cluster density was found to increase dramatically while the average cluster size decreased with the increase in the laser fluence. For a laser fluence of 70 J/cm^2, dome- shaped clusters that are smaller than the large huts formed at 23 J/cm^2 were observed. At a substrate temperature of 150 °C, misoriented three-dimensional (3D) clusters are formed producing only a RHEED background. At 400 and 500 °C, huts and a lower density of domes are formed, respectively. Above 600 °C, 3D clusters are formed on top of a discontinuous textured layer. © *2006 American Institute of Physics*. [DOI: 10.1063/1.2178679]

I. INTRODUCTION

The study of the self-assembled and self-organized nanostructures in heteroepitaxial systems is of much interest to achieve fundamental understanding of the properties of reduced-size condensed matter systems and for the development of quantum dot (QD)-based devices.[1,2] Self-assembled Ge QDs grown on Si are used in fabricating devices such as midinfrared photodetectors,[3–6] thermoelectric devices,[7] and enhanced performance Si solar cells.[8–10] From the basic physics point of view, Ge/Si is a model system for studying the growth dynamics of the Stranski-Krastanow (SK) mode. In such a system, growth starts by the formation of a two-dimensional (2D) wetting layer where the Ge film lattice constant adapts to that of the Si substrate.[1,2] However, due to the lattice mismatch of 4.2% between the film and the substrate, an elastic strain arises in the wetting layer, which increases linearly with the increase of the film thickness. When the thickness of the wetting layer reaches a critical value, which is estimated to be 4–6 ML (monolayer) (1 ML $=6.24\times10^{14}$ at./cm^2), the film relieves its internal strain by three-dimensional (3D) nucleation.[2] In the case of Ge on Si(100), 3D nucleation starts by the formation of {105}-faceted hut or pyramid clusters.[2] As the film coverage increases, multifaceted domes, faceted by {113} and {102} planes, develop on the expense of the hut clusters. With further increase in thickness, large clusters or superdomes start to appear.

Ge QDs were previously grown on Si(100) by molecular beam epitaxy (MBE),[11–16] chemical vapor deposition (CVD),[17,18] and liquid phase epitaxy (LPE).[19,20] The shape of the QDs was found to depend on the deposition technique as well as the deposition conditions. When Sb was used as a surfactant in the MBE growth of Ge/Si(100), the initial island shape changed from {105} faceted to {117} faceted.[21] When Ge was grown by liquid phase epitaxy, {115}-faceted islands were first observed instead of the {105}-faceted ones. As the coverage was increased, {111}-faceted pyramids were formed.[19,20] We have reported a preliminary study on pulsed laser deposition (PLD) of Ge on Si(100)-(2×1).[22] In the current work, we expand this study to include the effects of both substrate temperature and laser fluence on the growth dynamics and the produced QD morphology.

PLD is a powerful technique for growing thin films from the vapor phase. A high power pulsed laser is focused onto a target of the material to be grown. As a result, a plume of vaporized material is emitted and then collected on the substrate. Among its interesting features are the high preservation of stoichiometry,[23–25] its adaptability to grow multicomponent or multilayered films,[6,26] the ability to grow a thin film out of any material regardless of its melting point, the high energy of the ablated particles that may have beneficial effects on film properties, and PLD consists of periods of high deposition rate (on the microsecond time scale) followed by periods of no deposition (on the millisecond to the second time scale), allowing for surface relaxation that may lead to producing smoother films.[27] Producing large-area devices by PLD is a drawback of its use in industry. However, some experimental recipes of producing large-area wafers by PLD have been reported.[28,29]

Ge QDs have interesting midinfrared optical properties.[3,30] It was shown that the photoluminescence peak

[a)]Electronic mail: helsayed@odu.edu

of a single Ge QD dot layer changes from 1.3 to 1.6 μm with increasing thickness from 5 to 9 ML.[30] Such wavelength tunability is one of the reasons behind the great interest in Ge QD-based devices. Generally, QD-based devices consist of tens of multilayers of doped or undoped QDs separated by spacing layers. Apparently, the first two features of PLD make it a strong candidate for growing multilayered devices. In this case, only targets of different materials in the desired stoichiometry and doping are required without the need for residual gases or doping sources. In order to design efficient Ge QD-based devices by PLD, a clear understanding of how to control their physical properties through controlling the deposition parameters is required. The physical parameters of QDs depend strongly on their shape and size distribution, while the device quantum efficiency is affected by the density and spatial distribution of the QDs. Beside the substrate temperature, laser parameters (fluence, repetition rate, and wavelength) are unique controlling parameters of PLD. The density and size distribution of QDs are mainly controlled by both the deposition rate and adatoms' kinetic energy, which affects surface diffusion.[31] In the case of PLD, adatom surface diffusion is controlled by both the substrate temperature and the laser fluence, while deposition rate is mainly controlled by the laser fluence and the repetition rate. The spatial distribution depends on the homogeneity of the atomic flux, which is governed by the laser fluence. However, the dependence of the QD shape on deposition parameters has not been sufficiently explored for PLD. The current work aims to investigate the growth dynamics and the morphology of Ge QDs on Si(100)-(2×1).

II. EXPERIMENT

An ultrahigh vacuum chamber is used for deposition. The Si substrate is heated by direct current to obtain high temperatures. The Ge target is mounted on a rotated sample holder with a variable rotation speed. Target rotation during PLD minimizes the formation of particulates by exposing a fresh area to the laser. An Nd:YAG (yttrium aluminum garnet) laser (40 ns, 10 Hz) is used to ablate the Ge target. The laser is focused on the rotating target with a spot size of $\sim$330 μm (measured at $1/e$ of the peak value). The system is designed so that the laser is incident on the target at 45°. To monitor the deposition *in situ*, a 15 keV continuous electron gun is used to obtain RHEED patterns during growth. A phosphor screen is used to display the electron diffraction pattern, which is recorded by a charge coupled detector (CCD) camera.

The Si(100) samples are first cleaned by chemical etching using a modification to the Shiraki method.[32] The samples are dipped into a solution of H_2SO_4(97 wt %):H_2O_2(30 wt %)=4:1 (by volume) for 10 min, rinsed with ultrapure water for 10 min, then dipped into a solution of HF (50 wt %):H_2O=1:10 (by volume) for 1 min. The samples are loaded into the vacuum chamber within 5 min of chemical cleaning. The vacuum chamber is pumped down to $<1 \times 10^{-9}$ Torr. The chamber is baked at 300 °C for at least 12 h while the substrate is kept at 500 °C during the baking. When baking is completed, the sample is

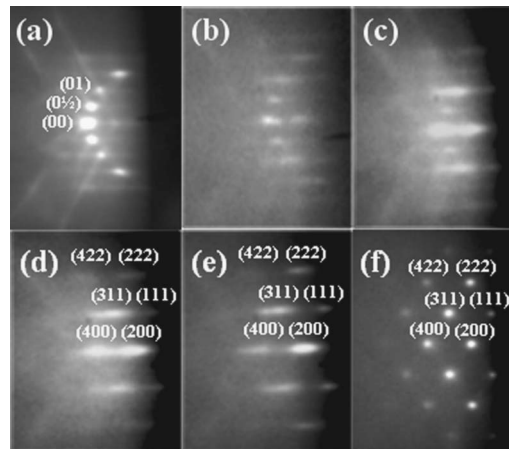FIG. 1. RHEED patterns taken at different thicknesses for deposition at 400 °C, 23 J/cm^2, 10 Hz. Substrate (2×1) reconstruction pattern is shown in (a). Growth started epitaxially, as seen in the RHEED pattern taken after the deposition of $\sim$3.3 ML shown in (b). At $\sim$4.1 ML, (c) elongated transmission features with lines at the position of the second order streaks started to appear. In the pattern at $\sim$6 ML (d), the lines disappeared while the elongation of the transmission features increased. As the thickness was increased, the transmission features became well defined and the elongation decreased, as observed in (e) taken at $\sim$9.3 ML. At $\sim$13 ML, the transmission features became more round (f).

kept at 800 °C for a few hours before being flashed to 1100 °C for about a minute. This procedure results in the observation of Si(100)-(2×1) reflection-high energy electron diffraction (RHEED) pattern.

Deposition takes place by focusing the laser beam onto the rotating Ge target, while the growth dynamics is studied by *in situ* RHEED. Later, the morphology of the grown films is studied by postdeposition atomic force microscopy (AFM). A series of films of different mean thicknesses was deposited at a substrate temperature of 400 °C using a laser of fluence of 23 J/cm^2 operating of 10 Hz. The growth dynamics and the morphology dependence on cluster size were studied. Another series of films was grown at 400 °C with different laser fluences in order to study the effect of the laser fluence. Finally, several 9 ML films were grown at different substrate temperatures.

III. RESULTS AND DISCUSSION

A. Growth dynamics

Ge films of different thicknesses were grown under the same deposition conditions (substrate temperature of 400 °C and a laser of fluence of 23 J/cm^2 operated at a repetition rate of 10 Hz). Thickness calibration was done in separate runs by placing a crystal thickness monitor at the substrate's location. Figure 1 shows a series of RHEED patterns as the film mean thickness was increased. The Si(100)-(2×1) diffraction pattern features, shown in Fig. 1(a), remained unchanged during the first few seconds of deposition in which the epitaxial growth of the wetting layer occurs. Figure 1(b) was taken at $\sim$3.3 ML, showing a RHEED pattern with equal streak spacing as in Fig. 1(a) but with reduced diffraction streak intensity. The epitaxial growth of the Ge wetting layer leads to a continuous increase in the lattice mismatch-induced internal strain as the film is grown. However, after
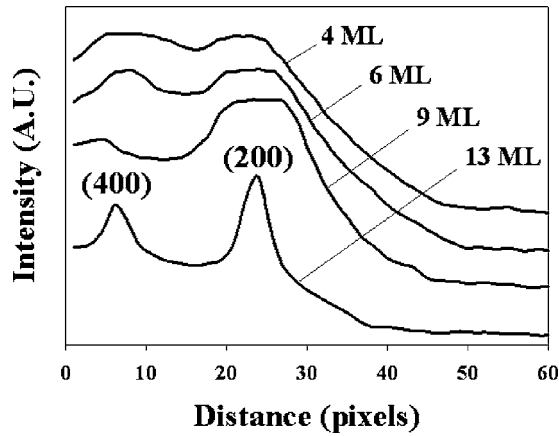
FIG. 2. Line profile measured along the (200)-(400) connecting line normal to the surface at different thicknesses. The transition from the elongated lines to sharp spots is shown.
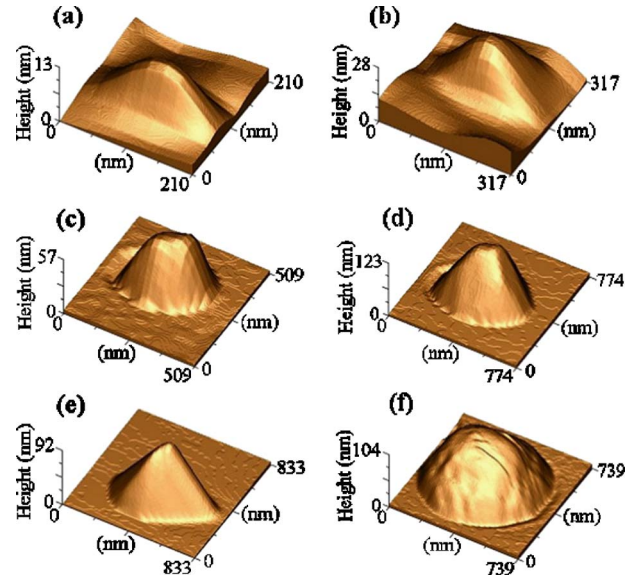

FIG. 3. (Color online) 3D AFM images of the clusters observed at different film thicknesses. Well-defined hut clusters observed at low thicknesses [(a) and (b)]. As the film thickness was increased huts became more round [(c) and (d)]. Some of these clusters grew into pyramids (e). The majority of clusters grew into domes (f).

depositing ~4 ML, elongated transmission features with lines at the positions of the second order strikes start to appear, as shown in Fig. 1(c). The appearance of such transmission features instead of the reflection ones indicates the beginning of the strain relief by the formation of 3D clusters. Elongated RHEED features result from transmission through asymmetric 3D clusters.[33,34] In the cases of growth by MBE and CVD, similar RHEED features were reported to correspond to the formation of {105}-faceted hut and pyramid clusters.[11,13,34] At ~6 ML, the lines at the positions of the second order strikes disappeared, while the elongated transmission features increased in intensity and elongation, as shown in Fig. 1(d). As the film thickness was increased, the transmission RHEED features split into well-defined features and their elongation started to decrease, as shown in Fig. 1(e) taken at ~9 ML. As the deposition continues, both the major (elongation) and minor lengths of the spot continued to decrease. Since the RHEED arrangement used probes an area of ~1 mm^2, such a decrease accounts for an increase in the Ge QDs' average size, within the limits of the electron penetration depth. This penetration depth is 15±4 nm in Ge at electron energy of 12 keV, as calculated by different inelastic mean free path (IMFP) models.[35,36] Both the transmission spots' major and minor lengths decreased with the increase in the film thickness and the spots became more round.

Figure 2 shows a set of line profiles taken at thicknesses corresponding to Figs. 1(c)–1(f). The line scans, which are taken normal to the surface and measured along the (200)–(400) connecting line, show the decrease in the spots' major length with film thickness. Such observation predicts a transition from an asymmetric cluster shape to a more symmetric one. Finally, the transmission features in the case of ~13 ML appear to be fully rounded, as shown in Fig. 1(f). Rounded spots result from transmission through rounded clusters. A similar spotty transmission pattern, with chevron lines due to the facetation of the Ge clusters, were observed when multifaceted "macroisland" clusters were formed (domes and superdomes faceted by {113} and {102} planes).[11,37] In our study, we did not observe chevron lines, which could be due to the lack of well-defined facets in the PLD-formed dome clusters.

Ex situ AFM was used to study the morphology of the Ge QDs and to correlate the morphology with the RHEED observations. Figure 3 shows 3D AFM images of the cluster shapes observed at the different film thicknesses. Depending on the film thickness, three cluster shapes are observed: huts, pyramids, and domes. Faceted hut clusters are observed to dominate at low film thicknesses with cluster sizes up to 400 nm and heights ranging up to 40 nm. Figures 3(a) and 3(b) show two representatives of these hut clusters. Figure 4 shows the analysis of some of the quantitative measurements performed on the clusters. The relation between the lateral aspect ratio (defined as major length/minor length) and the minor length of the clusters is shown in Fig. 4(a). Figure 4(b) shows the clusters' aspect ratio (i.e., the major length/height) as a function of their major lengths, while Fig. 4(c) shows the relation between the contact angle of the clusters' bounding planes with the Si(100) substrate. Small hut clusters are asymmetric in shape, as deduced from Fig. 4(a). The asymmetry decreases with the lateral size increase. From Fig. 4(b), it is observed that the aspect ratio decreases rapidly before leveling off asymptotically. In other words, for small clusters the rate of height increase is faster than that of lateral size increase. However, both rates become comparable as the cluster increases in size. This growth anisotropy may be attributed to the cluster's internal strain. Increasing the lateral size is expected to result in increasing the internal strain due to the lattice mismatch. On the contrary, increasing the cluster's height leads to more strain relief through the adjustment of the lattice spacing in the growing layers and therefore is favored over the lateral growth.[1] The contact angle increases linearly for clusters with heights less than 40 nm, as shown in Fig. 4(c). This leads to the continuous change of the planes faceting the clusters. For example, the huts shown in Figs. 3(a) and 3(b), are mainly faceted by planes having con-
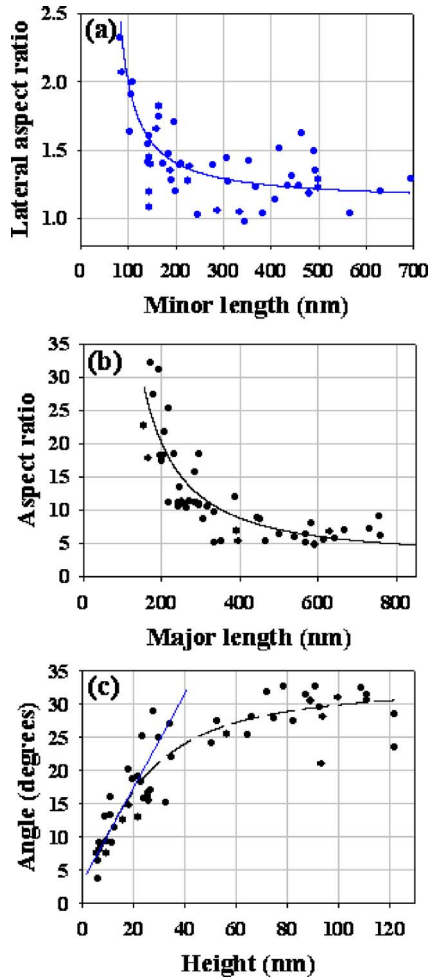
FIG. 4. (Color online) (a) Lateral aspect ratio of clusters (major length/minor length) as a function of the minor length. (b) Aspect ratio (major length/height) as a function of major length. (c) Contact angle that the bounding planes make with the substrate as a function of cluster's height.

tact angles of ~10° and ~18°, respectively, which account for the faceting planes of {811} and {310}.

For larger film thicknesses, the huts (of lateral sizes >400 nm) grew in size, became less defined, and lost their facetation. Figures 3(c) and 3(d) show two representatives of such clusters that are identified by their continuous round edges, indicating the lack of facetation. As they grew more in size, they became more laterally symmetric, as obtained from Fig. 4(a), in which the lateral aspect ratio asymptotically reached ~1.2. Figure 4(b) shows that the length-to-height ratio decreased approaching the asymptotic value of ~4. Thus, spherical cluster was not obtained under the considered deposition conditions. As for the slope of the clusters' edges, it asymptotically reached the value of ~31°, which assumes that both the height and the lateral size increased almost at the same rate.

With increased film thickness the hut clusters transformed into the domelike shape shown in Fig. 3(f), with length/height ratio of ~4. The smoothness of the dome, which could be seen as a continuous distribution of faceting planes, is noticeable. This morphology is consistent with the lack of observation of chevron lines in RHEED.[38] The chevron lines arise from the intersection of two diffraction patterns, each originating from one faceting plane.[34] However, a few numbers of pyramid clusters, Fig. 3(e), are observed among the domes. These pyramids are slightly elongated and their main faceting planes are the {305} with contact angles of ~31°.

The observation of huts that are faceted by different planes, depending on their size, has not been previously reported. Also, the observation of huts that are faceted by planes of large contact angles with the substrate differs from those reported in the cases of MBE, CVD, and LPE.[11,13,34] Another observation in the present PLD experiment is the formation of stable huts that are larger than those grown by the other deposition techniques. These observations could be attributed to PLD features, such as the high adatom energies, plume density, and the periodic nature.

B. Effect of laser fluence

Controlling thin film growth by changing the laser parameters, namely, fluence and repetition rate, is a unique feature of PLD. Figure 5 shows the AFM scans, 3D images of the QDs, and the resulting RHEED patterns obtained after depositing Ge on Si(100)-(2×1) for 80 s at 400 °C, 10 Hz but at different laser fluences (23, 47, and 70 J/cm²). For 23 J/cm², column (a), the origin of the elongated transmission streaks is the elongated hut clusters. Notice the low clusters' density in this case. When the laser fluence was increased to 47 J/cm², column (b), the cluster density increased while cluster sizes decreased. The 3D image of a representative cluster shows that the clusters became more symmetric in shape. This decreased the transmission RHEED streak elongation. When the fluence was increased to 70 J/cm², cluster density was seen to increase dramatically while the average size cluster decreased further. The shape of the clusters became almost symmetric, as seen in the 3D image, which resulted in round transmission RHEED spots. The cluster heights are much larger than those observed by other techniques.[17] The observation of domes for a laser fluence of 70 J/cm² that are smaller in size than the huts observed for a fluence of 23 J/cm² differs from other deposition methods. These observations show that the effect of the laser fluence is not only on the size and spatial distributions of the clusters but also on their morphology.

Figure 6 presents some statistics calculated from the above AFM scans. The number of clusters in the scanned area n the average cluster size d the coverage ratio θ, and the full width at half maximum (FWHM) of the distribution f are listed. With the increase of the laser fluence, the cluster density is seen to increase dramatically (from 3×10^7 cm^{-2} for 23 J/cm² to 1.3×10^8 and 6.3×10^8 cm^{-2} for 47 and 70 J/cm², respectively), while the average cluster size decreased (~362, 287, and 107 nm for 23, 47, and 70 J/cm², respectively). One may notice that the cluster density is at least an order of magnitude less than that observed in other deposition techniques under standard deposition conditions,[8,18,39] which could be attributed to the higher kinetic energy of the adatoms in the case of PLD. The dependence of the FWHM of the size distribution on the laser fluence is complicated. It is known that on samples with
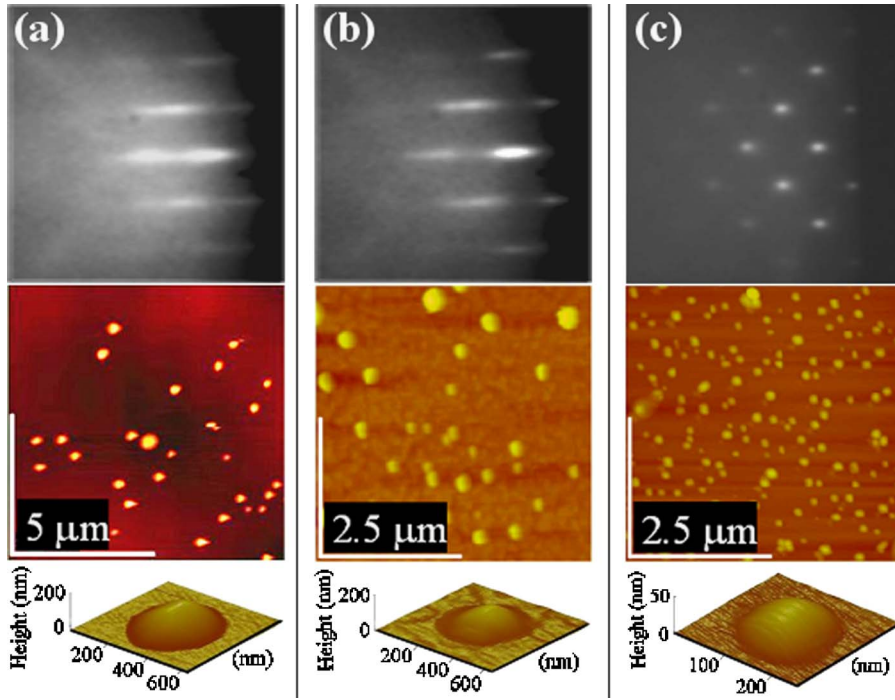
FIG. 5. (Color online) RHEED patterns, AFM scans, and 3D AFM scans of three samples deposited at 400 °C, 10 Hz, and column (a) 23 J/cm², column (b) 47 J/cm², and column (c) 70 J/cm².

different cluster shapes, each cluster shape has its own size distribution. This is the reason for the bimodal distributions observed in some systems.[17,40,41] The shapes of the clusters are different in these three cases. However, one may easily see that films prepared at 70 J/cm² have the narrowest distribution.

In vapor phase deposition, the nucleation density and the clusters' sizes are determined through the competition between the atomic flux F (atoms/area × time) and adatoms' diffusion coefficient D (area/time), given as $D = D_0 \exp[E_d/k_B T]$, with E_d as the diffusion barrier.[31,42] The density of stable islands is given by[43,44]

$$N = \eta(\Theta)(D_0/F)^{-\chi} \exp\left(-\frac{\chi E_d}{k_B T}\right), \qquad (1)$$

with $\eta(\Theta) \cong \Theta^{1/3}$ as the coverage Θ dependent factor and χ as the scaling factor. Therefore, a high flux results in the high supersaturation of adatoms leading to a large nucleation density of small clusters. On the other hand, high substrate temperatures increase the adatom diffusion coefficient favoring the formation of low density of larger clusters. In PLD, the nucleation density is expected to be dependent on the laser's repetition rate and pulse duration in addition to the parameters in Eq. (1). Rate equations were solved numerically and the number of stable islands was found as a function of D/F for the case of PLD for different deposition durations and laser repetition rates and was compared to the case of MBE.[44] According to these models, both MBE and PLD result in the same island density N for very low values of D/F, while PLD yields higher values of N for larger D/F.

The effect of the laser fluence on nucleation density is complex since changing the laser fluence affects both the atom flux F and the kinetic energy of the ablated species,[45] which range from 0.1 to 1000 eV. Therefore, the diffusion coefficient D is expected to depend on the particles' kinetic

energy as well as the substrate temperature. Moreover, the effect of the particles' kinetic energy on D is further complicated by the interaction between the incident particles and the adatoms.[46] Although the functional dependence of F on the laser fluence is not known, it is not expected to be linear, since increasing the fluence results in increasing the ablation yield and a more directional plume.[45]

One model showed that the growth behaviors of PLD and MBE are equivalent at very small plume intensities I, which is the plume intensity in units of atoms/area.[31,47] In this regime, the nucleation density follows the relation $N \propto (D/F)^{-\gamma}$ and, therefore, depends on the laser fluence through the competition between D and F, since they are both functions of I. The exponent γ is a positive constant, the value of which depends on the nucleation and growth mechanisms. However, above a certain critical intensity I_c PLD shows no dependence on F and D but rather on I according to the relation $N \propto I^\nu$, with ν as some exponent.[31,47] The reason for the change in behavior at I_c is that the huge number of deposited atoms in each pulse leads to high nucleation probability before even the effects of the change in D and F take place. Therefore, the nucleation density in the case of PLD may be formulated intuitively as[31]

$$N \propto (D/F)^{-\gamma} f(I/I_c), \qquad (2)$$

where

$$f(I/I_c) \sim \begin{cases} \text{const}, & I \ll I_c \\ (I/I_c)^\nu, & I_c \gg I. \end{cases} \qquad (3)$$

Therefore, increasing the plume intensity, through increasing the laser fluence, acts to increase the nucleation density. The drawback of this model is the assumption that atoms are deposited at thermal energies, which is not the case in PLD. However, it gives a decent picture of how the nucleation
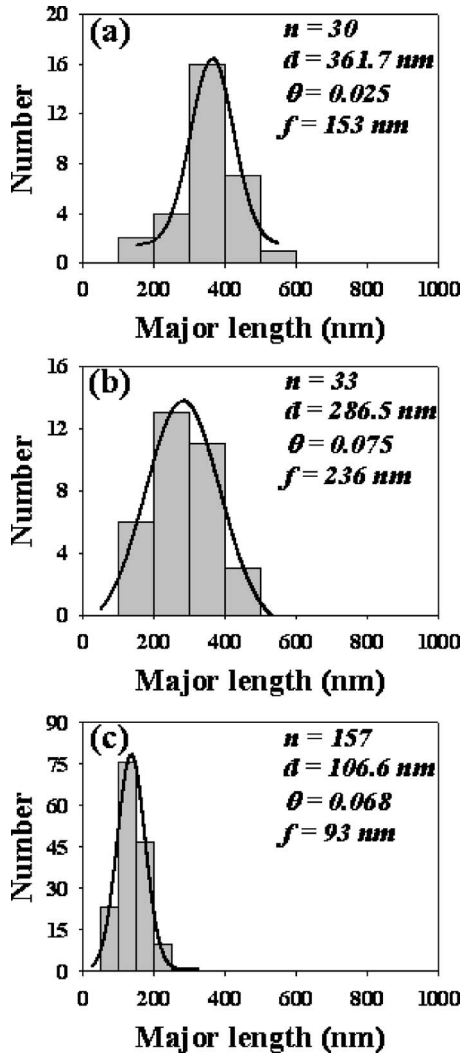
FIG. 6. Size distributions of the clusters formed on three different samples deposited at 400 °C, 10 Hz, and column (a) 23 J/cm², column (b) 47 J/cm², and column (c) 70 J/cm². The number of clusters in the scanned area n, the average cluster size d, the coverage ratio θ, and the full width at half maximum (FWHM) of the distribution f are listed.

density and the average cluster size are dependent on D, F, and I.

Because of the current lack of understanding of the dependence of F, kinetic energy distribution, and I on the laser fluence, the dependence of the cluster density and average cluster size on the laser fluence is not well explained. In our current situation, if we assume that the studied laser fluences result in plume intensities above the critical value (i.e., $I > I_c$), the nucleation density will be a power function of the intensity. If this is not the case (i.e., $I < I_c$), the increase in the density with the laser fluence indicates that the effect of the increase in the plume density overwhelms that due to the increase in adatoms' kinetic energy.

C. Effect of substrate temperature

Figure 7 shows the RHEED patterns obtained after the deposition of ∼9 ML of Ge on Si(100)-(2×1) at different substrate temperatures along with the pattern obtained from the substrate before deposition. Figure 8 shows the AFM scans corresponding to the samples of Fig. 7. For growth at
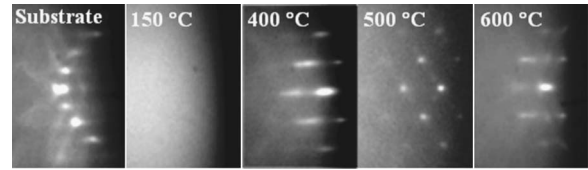

FIG. 7. RHEED patterns of different samples ∼9 ML thick deposited at 23 J/cm², 10 Hz, and different substrate temperatures.

150 °C, the (2×1) diffraction pattern becomes dimmer continuously during the growth of the Ge film resulting in the shown diffused pattern indicating that the grown clusters are misoriented. The AFM imaging of this sample, Fig. 8(a), shows the formation of randomly distributed 3D clusters, which produces the diffuse RHEED pattern in Fig. 7. Similar results were observed for the Si homoepitaxy at low temperatures.[32] For deposition at 400 °C, the formation of elongated hut clusters was observed as shown in Fig. 8(b). These clusters give the elongated transmission RHEED pattern shown in Fig. 7. The RHEED transmission pattern with rounded spots obtained for deposition at 500 °C indicates the formation of dome clusters as shown in the AFM in Fig. 8(c). Comparing AFM images in Figs. 8(b) and 8(c) shows the effect of the substrate temperature on the cluster morphology, nucleation density, and cluster spatial distribution. The cluster morphology changed from the asymmetric hut shape to the symmetric dome shape. The decrease in the cluster density is consistent with the general behavior described by Eq. (2), in which the nucleation density decreases with the increase of the diffusion coefficient due to the increase in temperature. For growth at 600 °C a transmission RHEED pattern is seen on top of broken rings, as shown in Fig. 7. The incomplete concentric rings usually results from textured structures, i.e., surfaces with domains that have a distribution of orientations but are largely near one value.[48,49] Figure 8(d) is the AFM image corresponding to the sample grown at 600 °C, which shows 3D clusters formed on top of a discontinuous layer.
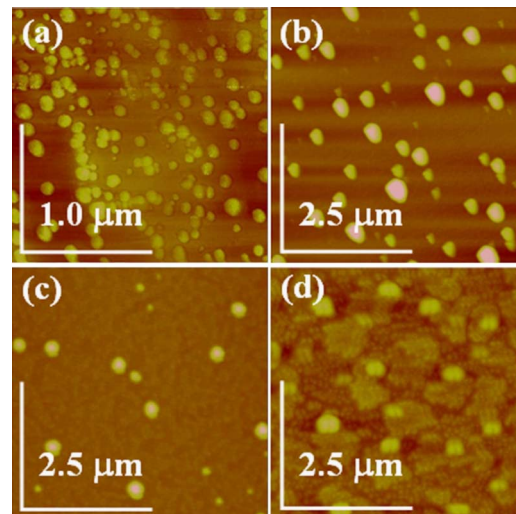

FIG. 8. (Color online) AFM scans corresponding to the samples of Fig. 5: (a) 150 °C, (b) 400 °C, (c) 500 °C, and (d) 600 °C.

IV. CONCLUSION

The growth dynamics and the morphology of Ge QDs grown on Si(100)-(2×1) by PLD were studied by RHEED and AFM. After the completion of the wetting layer, Ge was observed to form hut clutters faceted by planes having contact angles with the substrate that increase with the height of the cluster. As the cluster size increased with further deposition, they lost their facetation and became rounded forming a dome shape. The effect of the laser fluence on the growth dynamics and cluster morphology was studied. As the laser fluence was increased, the clusters' density increased dramatically, while the average cluster sizes were reduced. At a substrate temperature of 150 °C, misaligned clusters formed giving a diffuse RHEED pattern. At 400 and 500 °C, transmission RHEED patterns were observed indicating the growth of oriented clusters. Around 600 °C, the QDs were formed on top on textured surfaces.

ACKNOWLEDGMENTS

[1] C. Teichert, Phys. Rep. **365**, 335 (2002).

[2] B. Voigtländer, Surf. Sci. Rep. **43**, 127 (2001).

[3] V. A. Egorov *et al.*, Phys. Solid State **46**, 49 (2004).

[4] A. Elfving, G. V. Hansson, and W.-X. Ni, Physica E (Amsterdam) **16**, 528 (2003).

[5] M. Elkurdi *et al.*, Physica E (Amsterdam) **16**, 450 (2003).

[6] M. S. Hegazy, T. F. Refaat, M. Nurul Abedin, and H. E. Elsayed-Ali, Opt. Eng. (Bellingham) **44**, 59702 (2005).

[7] J. L. Liu, A. Khitun, K. L. Wang, T. Borca-Tasciuc, W. L. Liu, G. Chen, and D. P. Yu, J. Cryst. Growth **227–228**, 1111 (2001).

[8] A. Alguno, N. Usami, T. Ujihara, K. Fujiwara, G. Sazaki, K. Nakajima, and Y. Shiraki, Appl. Phys. Lett. **83**, 1258 (2003).

[9] H. Presting, J. Konle, H. Kibbel, and F. Banhart, Physica E (Amsterdam) **14**, 249 (2002).

[10] J. Knole, H. Presting, and H. Kibbel, Physica E (Amsterdam) **16**, 596 (2003).

[11] V. Cimalla, K. Zekentes, and N. Vouroutzis, Mater. Sci. Eng., B **88**, 186 (2002).

[12] I. Goldfarb, P. T. Hayden, J. H. G. Owen, and G. A. D. Briggs, Phys. Rev. Lett. **78**, 3959 (1997).

[13] Y.-W. Mo, D. E. Savage, B. S. Swartzentruger, and M. G. Lagally, Phys. Rev. Lett. **65**, 1020 (1990).

[14] A. I. Nikiforov, V. A. Cherepanov, O. P. Pchelyakov, A. V. Dvurechenskii, and A. I. Yakimov, Thin Solid Films **380**, 158 (2000).

[15] O. P. Pchelyakov, V. A. Markov, A. I. Nikiforov, and L. V. Sokolov, Thin Solid Films **306**, 299 (1997).

[16] J. A. Floro, E. Chason, L. B. Freund, R. D. Twesten, R. Q. Hwang, and G. A. Lucadamo, Phys. Rev. B **59**, 1990 (1999).

[17] T. I. Kamins, E. C. Carr, R. S. Williams, and S. J. Rosner, J. Appl. Phys. **81**, 211 (1997).

[18] P. S. Chen, Z. Pei, Y. H. Peng, S. W. Lee, and M.-J. Tsai, Mater. Sci. Eng., B **108**, 213 (2004).

[19] M. Schmidbauer, T. Wiebach, H. Raidt, M. Hanke, R. Köhler, and H. Wawre, Phys. Rev. B **58**, 10523 (1998).

[20] W. Dorsch, S. Christiansen, M. Albrecht, P. O. Hansson, E. Bauser, and H. P. Strunk, Surf. Sci. **331–333**, 896 (1995).

[21] M. Horn-von Hoegen, B. H. Müller, A. Al Falou, and M. Henzler, Phys. Rev. Lett. **71**, 3170 (1993).

[22] M. S. Hegazy and H. E. Elsayed-Ali, Appl. Phys. Lett. **86**, 343104 (2005).

[23] B. Dam, J. Rector, M. F. Chang, S. Kars, D. G. de Groot, and R. Griessen, Appl. Phys. Lett. **65**, 1581 (1994).

[24] Y. Iijima, K. Kakimoto, and T. Saitoh, IEEE Trans. Appl. Supercond. **13**, 2466 (2003).

[25] K. Develos-Bagarinao, H. Yamasaki, Y. Nakagawa, and K. Endo, Physica C **412–414**, 1286 (2004).

[26] A. Ohtomo and A. Tsukazaki, Semicond. Sci. Technol. **20**, S1 (2005).

[27] P. P. Pronko, Z. Zhang, and P. A. VanRompay, Appl. Surf. Sci. **9643**, 1 (2003).

[28] M. Lorenz *et al.*, IEEE Trans. Appl. Supercond. **11**, 3209 (2001).

[29] B. Schey, T. Bollmeier, M. Kuhn, W. Biegel, and B. Stritzker, Rev. Sci. Instrum. **69**, 474 (1998).

[30] K. Brunner, Rep. Prog. Phys. **65**, 27 (2002).

[31] B. Hinnemann, H. Hinrichsen, and D. E. Wolf, Phys. Rev. Lett. **87**, 135701 (2001).

[32] M. S. Hegazy and H. E. Elsayed-Ali, J. Vac. Sci. Technol. A **20**, 2068 (2002).

[33] W. Braun, *Applied RHEED* (Springer-Verlag, Berlin, 1999).

[34] C. E. Aumann, Y.-W. Mo, and M. G. Lagally, Appl. Phys. Lett. **59**, 1061 (1991).

[35] M. P. Seah and W. A. Dench, Surf. Interface Anal. **1**, 2 (1979).

[36] C. J. Powell, A. Jablonski, I. S. Tilinin, S. Tanuma, and D. R. Penn, J. Electron Spectrosc. Relat. Phenom. **98–99**, 1 (1999).

[37] J. W. Lee, D. Schuh, M. Bichler, and G. Abstreiter, Appl. Surf. Sci. **228**, 306 (2004).

[38] M. D. Kim, T. W. Kim, and Y. D. Woo, J. Cryst. Growth **265**, 41 (2004).

[39] S. W. Lee, L. J. Chen, P. S. Chen, M.-J. Tsai, C. W. Liu, W. Y. Chen, and T. M. Hsu, Appl. Surf. Sci. **224**, 152 (2004).

[40] S. Anders, C. S. Kim, B. Klein, M. W. Keller, R. P. Mirin, and A. G. Norman, Phys. Rev. B **66**, 125309 (2002).

[41] V. Le Thanh, P. Boucaud, D. De Débarre, and Y. Zheng, Phys. Rev. B **58**, 211 (1998).

[42] Z. Zhang and M. G. Lagally, Science **276**, 377 (1997).

[43] J. Shen, Z. Gai, and J. Kirschner, Surf. Sci. Rep. **52**, 163 (2004).

[44] P.-O. Jubert, O. Fruchart, and C. Meyer, Surf. Sci. **552**, 8 (2003).

[45] N. N. Nedialkov, P. A. Atanasov, S. E. Imamova, A. Ruf, P. Berger, and F. Dausinger, Appl. Phys. A: Mater. Sci. Process. **79**, 1121 (2004).

[46] D. M. Zhang, L. Guan, Z. H. Li, G. J. Pan, H. Z. Sun, X. Y. Tan, and L. Li, Surf. Coat. Technol. **200**, 4027 (2006).

[47] B. Hinnemann, H. Hinrichsen, and D. E. Wolf, Phys. Rev. E **67**, 11602 (2003).

[48] D. Litvinov, T. O'Donnell, and R. Clarke, J. Appl. Phys. **85**, 2151 (1999).

[49] S. Andrieu and P. Frechard, Surf. Sci. **360**, 289 (1996).